Progress In Electromagnetics Research, PIER 62, 143–164, 2006

MODELLING THE PASSIVE MICROWAVE REMOTE SENSING OF WET SNOW

Z.-X. Li

Electromagnetic Academy at Zhejiang University
Hangzhou, Zhejiang, China, 310075

Abstract—Combined volume scattering with rough surface scattering effects in passive microwave remote sensing of wet snow is studied in this paper. The dense medium radiative transfer (DMRT) theory with quasicrystalline approximation (QCA) is used to describe the volume scattering model for densely distributed sticky coated dielectric particles. The Numerical Maxwell Model of 3D simulations (NMM3D) is used to simulate the rough surface bistatic scattering and emission, and the bistatic scattering coefficients and emissivity of the rough surfaces are utilized as the boundary conditions for the DMRT. Full multiple scattering solutions are calculated by solving the DMRT numerically. Wet snow model is adopted in this paper, the results are illustrated for a layer of wet snow over a moist rough ground at 18.7 GHz and 38.5 GHz.

1. INTRODUCTION

In microwave remote sensing of snow, there are volume scattering from the ice grains and surface scattering of the interface between snow and the ground. The combined volume and surface scattering were treated by classical radiative transfer theory with rough surface boundary conditions based on physical optics or small perturbation methods in the past [1, 2].

The two effects are combined by using the DMRT with rough surface boundary conditions of NMM3D [3] in this paper. For volume scattering, the DMRT is used based on the QCA for sticky coated dielectric particles that can be of moderate size compared with wavelength. The DMRT theory includes the effects of correlated scattering and coherent field interaction in the near and intermediate field range [4]. For rough surface scattering, in the past, analytic methods such as Kirchhoff approximation or small perturbation

method [1, 2] were utilized. However, with the advances of more powerful computers and more efficient computation methods, we calculate the rough surface effects through numerical solutions of three dimensional Maxwell equations. The NMM3D simulations are based on the sparse matrix canonical grid method (SMCG), which is a fast method of solving the matrix equation associated with the method of moments [3]. The Gaussian random rough surfaces with exponential correlation functions are used because they are more applicable to land surfaces than Gaussian correlation function [5]. The Rao-Wilton-Glisson (RWG) basis functions are used in NMM3D to improve the accuracy of the solution particularly in relation to energy conservation [5].

In order to simulate remote sensing of wet snow, effective permittivity of wet snow is important to be exactly known, which has ever been calculated by strong fluctuation theory in recently year [6], to effectively describe the wet snow model, the dense medium with coated particles is considered in this paper. The coated particle consists of two layers within each the permittivity is constant [7]. For a medium with densely distributed coated particles, such as melting snow, wet snow and composite materials with coated granules, the model can be used to study waves propagating within it.

In Section 2, the DMRT theory, the rough surface boundary conditions and the bistatic coefficients of rough surface scattering obtained by NMM3D incorporated in rough surface boundary conditions for DMRT for passive microwave remote sensing of wet snow are described. Meanwhile, effective propagation constants and attenuation rates in media with densely distributed coated dielectric particles pertinent to wet snow are introduced. In Section 3, results for passive microwave remote sensing at 18.7 GHz and 38.5 GHz of a layer of wet snow overlying a rough moist soil ground are illustrated. In order to study rigorously the frequency dependence of microwave signatures, the same set of physical parameters of grain sizes, fractional volumes, and rough surface rms height and correlation lengths for both 18.7 GHz and 38.5 GHz is used to calculate the brightness temperatures.

2. METHODOLOGY

2.1. Dense Media Radiative Transfer Model for Volume Scattering

In the DMRT model for wet snow, the sticky coated dielectric particle model is used, where the snow grains are allowed to stick together to form clusters. Distinguishing features of the dense media model are: first, although the particles are small compared with wavelength,

due to the aggregate nature of the sticky particles, the frequency dependence of volume scattering is weaker than that by classical Rayleigh prediction of frequency to the fourth power. Secondly, the mean cosine of the scattering is not equal to zero in contrast to the classical Rayleigh phase matrix. The pair distribution functions of sticky particles are used [3, 5].

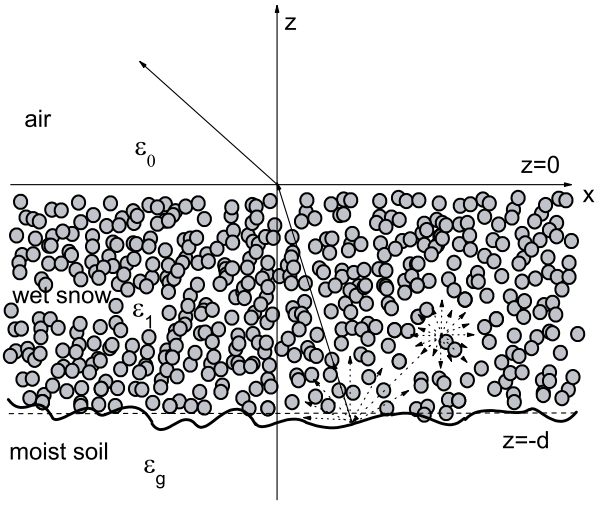

Figure 1. Geometry of the problem for simulations with DMRT model.

For the wet snow layer overlying ground with a rough moist soil surface under consideration, it was modeled by a slab of densely-distributed sticky spherical ice coated with thin water film and embedded in a background medium of permittivity ε_0 (air)(Fig. 1). Its effective permittivity is ε_1. The layer thickness is d. The moist soil has a permittivity $\varepsilon_g = \varepsilon_g' + \varepsilon_g''$. The DMRT equations for passive remote sensing are in the following form [2]:

$$\cos\theta \frac{d\overline{I}_u(z,\theta)}{dz} = -\kappa_e \overline{I}_u(z,\theta) + \int_0^{\frac{\pi}{2}} d\theta' \sin\theta' \cdot \overline{\overline{P}}(\theta,\theta') \cdot \overline{I}_u(z,\theta') + \int_0^{\frac{\pi}{2}} d\theta' \sin\theta' \cdot \overline{\overline{P}}(\theta,\pi-\theta') \cdot \overline{I}_d(z,\theta') + \kappa_a \cdot C\overline{T} \quad (1)$$

$$-\cos\theta \frac{d\overline{I}_d(z,\theta)}{dz} = -\kappa_e \overline{I}_d(z,\theta) + \int_0^{\frac{\pi}{2}} d\theta' \sin\theta' \cdot \overline{\overline{P}}(\pi-\theta,\theta') \cdot \overline{I}_u(z,\theta') + \int_0^{\frac{\pi}{2}} d\theta' \sin\theta' \cdot \overline{\overline{P}}(\pi-\theta,\pi-\theta') \cdot \overline{I}_d(z,\theta') + \kappa_a \cdot C\overline{T} \quad (2)$$

where $\overline{I}_u(z,\mu_i) = \begin{bmatrix} \overline{I}_u^v(z,\mu_i) \\ \overline{I}_u^h(z,\mu_i) \end{bmatrix}$, $\overline{I}_d(z,\mu_i) = \begin{bmatrix} \overline{I}_d^v(z,\mu_i) \\ \overline{I}_d^h(z,\mu_i) \end{bmatrix}$, v and h are, respectively, the vertical and horizontal polarization directions of the incident wave, T is snow's brightness temperature, κ_e, κ_a, $\overline{\overline{P}}$ are snow's extinction rate, absorbing coefficient and phase matrix respectively [3, 8, 9]. They are calculated by using QCA theory. Using the same theory, the effective propagation constant of wet snow is calculated, which depends on fractional volume, diameter and permittivity of the water-coated ice. The effective permittivity ε_1 of wet snow is equal to the square of the ratio of its effective propagation constant to the propagation constant of air. Upon discretation using Gaussian Legendre Quadrature in the discrete ordinate-eigenanalysis method, the DMRT equation can be approximated by a quadrature formula as follows

$$\begin{aligned} \overline{\overline{\mu}}\frac{d\overline{I}_u(z,\mu)}{dz} &= -\overline{\overline{\kappa_e}}\cdot\overline{I}_u(z,\mu) + \overline{\overline{\alpha}}\cdot\overline{\overline{P}}(\mu,\mu')\cdot\overline{I}_u(z,\mu') \\ &\quad +\overline{\overline{\alpha}}\cdot\overline{\overline{P}}(\mu,-\mu')\cdot\overline{I}_d(z,-\mu') + \kappa_a\cdot C\overline{T} \qquad (3) \\ \overline{\overline{\mu}}\frac{d\overline{I}_d(z,\mu)}{dz} &= -\overline{\overline{\kappa_e}}\cdot\overline{I}_d(z,\mu) + \overline{\overline{\alpha}}\cdot\overline{\overline{P}}(-\mu,\mu')\cdot\overline{I}_u(z,\mu') \\ &\quad +\overline{\overline{\alpha}}\cdot\overline{\overline{P}}(-\mu,-\mu')\cdot\overline{I}_d(z,-\mu') + \kappa_a\cdot C\overline{T} \qquad (4) \end{aligned}$$

where

$$\overline{\overline{\mu}} = \begin{bmatrix} \overline{\overline{\mu_v}} & 0 \\ 0 & \overline{\overline{\mu_h}} \end{bmatrix}, \quad \overline{\overline{\mu_{v/h}}} = \begin{bmatrix} \mu_1 & & & & \\ & \mu_2 & & & \\ & & \ddots & & \\ & & & \mu_i & \\ & & & & \ddots \\ & & & & & \mu_N \end{bmatrix}, \quad \mu_i = \cos\theta_i,$$

$i = 1, \ldots, N$, α_i is the Christoffel weighting functions. There are $2N$ μ_i values and $2N$ α_i value, $\mu_i = -\mu_{-i}$, $\alpha_i = \alpha_{-i}$.

At the surface between snow and air ($z = 0$), the boundary condition is

$$\overline{I}_d(\mu, z=0) = \overline{\overline{r_{10}}}\cdot\overline{I}_u(\mu, z=0) \qquad (5)$$

where $\overline{\overline{\mu}} = \begin{bmatrix} \overline{\overline{r_v}} & 0 \\ 0 & \overline{\overline{r_h}} \end{bmatrix}$ is the flat surface's reflectivity.

At the rough surface of soil ($z = -d$), the boundary condition is

$$\overline{I}_u(\theta, z=-d)\cdot\cos\theta = \overline{\overline{\gamma_c}}\cdot\overline{I}_d(\theta', z=-d)\cdot\cos\theta$$

$$+\int_0^{\frac{\pi}{2}} d\theta \sin\theta \cdot \int_0^{2\pi} d\varphi' \overline{\overline{\gamma_{ic}}}(\theta,\varphi,\theta',\varphi') \cdot \cos\theta' \cdot \overline{I}_d(\theta', z=-d) + \overline{\overline{e}}(\theta) T_g \cos\theta \tag{6}$$

where $\overline{\overline{\gamma_c}} = \begin{bmatrix} \overline{\overline{\gamma_c^v}} & 0 \\ 0 & \overline{\overline{\gamma_c^h}} \end{bmatrix}$ and $\overline{\overline{\gamma_{ic}}} = \begin{bmatrix} \overline{\overline{\gamma_{ic}^{vv}}} & \overline{\overline{\gamma_{ic}^{vh}}} \\ \overline{\overline{\gamma_{ic}^{hv}}} & \overline{\overline{\gamma_{ic}^{hh}}} \end{bmatrix}$ are the coherent and incoherent bistatic scattering coefficients of rough surfaces. $\overline{\overline{e}} = \begin{bmatrix} \overline{\overline{e_v}} & 0 \\ 0 & \overline{\overline{e_h}} \end{bmatrix}$ is thermal emissivity of the rough soil surface, and T_g is soil's brightness temperature.

We set

$$\overline{\overline{\Gamma_{ic}}}(\theta,\theta') = \int_0^{2\pi} d\varphi \overline{\overline{\gamma_{ic}}}(\theta,\varphi,\theta',\varphi'=0) \tag{7}$$

$$\begin{aligned} &\cos\theta \cdot \overline{I}_u(\theta, z=-d) = \cos\theta \cdot \overline{\overline{\gamma_c}}(\theta) \cdot \overline{I}_d(\theta, z=-d) \\ &+\int_0^{2\pi} d\theta \sin\theta \overline{\overline{\Gamma_{ic}}}(\theta,\theta') \cdot \cos\theta' \cdot \overline{I}_d(\theta, z=-d) + \overline{\overline{e}}(\theta) \cdot T_g \cos\theta \end{aligned} \tag{8}$$

Applying discrete ordinate-eigenanalysis method, the rough surface scattering boundary condition equation can be approximated by a quadrature formula as follow

$$\begin{aligned} \overline{I}_u(\mu, z=-d) \;=\; &\left(\overline{\overline{r_c}}(\mu) + \overline{\overline{\mu}}^{-1} \cdot \overline{\overline{\alpha}} \cdot \overline{\overline{\Gamma_{ic}}}(\mu,\mu') \cdot \overline{\overline{\mu'}}\right) \cdot \overline{I}_d(\mu, z=-d) \\ &+\overline{\overline{e}}(\mu) \cdot T_g \end{aligned} \tag{9}$$

Define

$$\overline{\overline{r_g}}(\mu, z=-d) = \left(\overline{\overline{r_c}}(\mu) + \overline{\overline{\mu}}^{-1} \cdot \overline{\overline{\alpha}} \cdot \overline{\overline{\Gamma_{ic}}}(\mu,\mu') \cdot \overline{\overline{\mu'}}\right) \tag{10}$$

yields

$$\overline{I}_u(\mu, z=-d) = \overline{\overline{r_g}}(\mu, z=-d) \cdot \overline{I}_d(\mu, z=-d) + \overline{\overline{e}}(\mu) \cdot T_g \tag{11}$$

2.2. Numerical Implementation of Rough Surface Boundary Conditions

A tapered plane wave [3, 5] impinging from wet snow onto the moist ground is considered in Fig. 2. The ground and snow interface has a random height profile. The incident electromagnetic wave is tapered so that the illuminated rough surface can be confined to a finite size. Numerical simulations of Maxwell equations are performed by the NMM3D, in which the PMCHW formulation with RWG basis functions is used [3, 5], and the SMCG fast matrix solver is adopted.

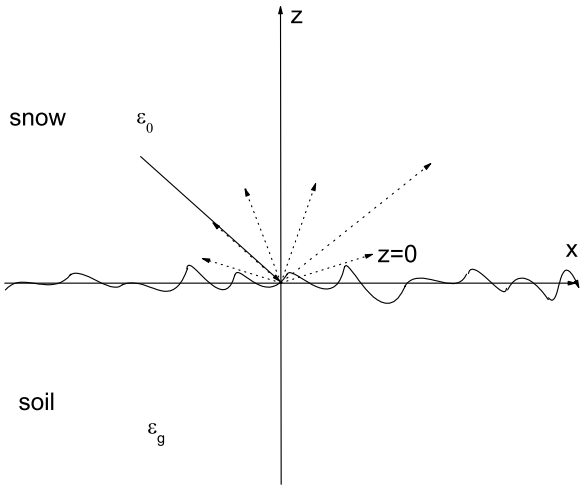

Figure 2. Geometry of the rough surface problem for simulations with NMM3D model.

The bistatic scattering coefficients are normalized by the incident power by using NMM3D, which are subsequently used in the boundary conditions of DMRT model. The bistatic scattering coefficients are [3],

$$\gamma_{\alpha\beta}(\theta_s, \varphi_s; \theta_i, \varphi_i) = \frac{\left|\overline{E}_\alpha^s\right|}{2\eta_1 P_\beta^{inc}} \tag{12}$$

where α and β are the polarizations of the scattering and incident wave, respectively.

Unlike infinite surfaces, the coherent scattering from finite surfaces is bistatic. In the simulations, the coherent bistatic scattering coefficients from the finite surface are calculated by

$$\gamma_{\alpha\beta}^c(\theta_s, \varphi_s; \theta_i, \varphi_i) = \frac{\left|\left\langle \overline{E}_\alpha^s \right\rangle\right|}{2\eta_1 P_\beta^{inc}} \tag{13}$$

where $\langle\ \rangle$ denotes ensemble average over realizations. Incoherent bistatic coefficients from the finite surface are next calculated by subtracting the coherent scattering from the total scattering

$$\gamma_{\alpha\beta}^{ic}(\theta_s, \varphi_s; \theta_i, \varphi_i) = \gamma_{\alpha\beta}(\theta_s, \varphi_s; \theta_i, \varphi_i) - \gamma_{\alpha\beta}^c(\theta_s, \varphi_s; \theta_i, \varphi_i) \tag{14}$$

To obtain the coherent reflectivity for "infinite" surface, the coherent bistatic scattering coefficients of finite surfaces over scattered angles is

integrated. The *coherent reflectivity* at incident angle (θ_i, φ_i) is

$$\gamma_c(\theta_i, \varphi_i) = \int_0^{\frac{\pi}{2}} \sin\theta_s d\theta_s \int_0^{2\pi} d\varphi_s \gamma^c_{\alpha\beta}(\theta_s, \varphi_s; \theta_i, \varphi_i) \tag{15}$$

Emissivity of the rough surface at incident angle (θ_i, φ_i) is transmissivity, which by reciprocity and energy conservation, is equal to

$$e_\alpha(\theta_i, \varphi_i) = 1 - \int_0^{\frac{\pi}{2}} \sin\theta_s d\theta_s \int_0^{2\pi} d\varphi_s \left(\gamma_{h\alpha}(\theta_s, \varphi_s; \theta_i, \varphi_i) + \gamma_{v\alpha}(\theta_s, \varphi_s; \theta_i, \varphi_i)\right) \tag{16}$$

When applying discrete ordinate-eigenanalysis method to the DMRT equations (3) and (4) and rough surface boundary condition equation (11), α_i, $\mu_{i(i=1,\ldots,N)}$ will be used. In general, the choice of the order of quadrature N is dependent on the angular variation of the integrand. $N = 16$ is commonly chosen in the simulations. There are 16 incident angles (θ_i, φ_i). Assuming azimuthal symmetry, we can take φ_i equal to 0. For each θ_i, $\gamma^{ic}_{\alpha\beta}(\theta_s, \varphi_s; \theta_i, \varphi_i = 0)$ owns 16 θ_s and many φ_s. Then we use integration over φ_s to get $\overline{\overline{\Gamma_{ic}}}(\theta_s, \theta_i)$ as indicated in Eq. (7). The surface area needs to increase when the incident angle increases [5]. In the simulations a surface of area 8 wavelengths by 8 wavelengths is used, which is not large enough when the incident angle exceeds 60 degrees. However, since the forward scattering in the specular direction dominates and resembles that of flat surface when the incident angle is large, for incident angle larger than 60°, flat surface results are used for the boundary conditions of the transfer equation.

2.3. Effective Propagation Constants and Attenuation Rates in Media of Densely Distributed Coated Dielectric Particles for Wet Snow Model

In general, a numerical technique is required to solve for the effective propagation constants when particle sizes are comparable to or large than wavelength. The case of moderate size coated particles (Fig. 3) will be illustrated using the quasi-crystalline approximation in this section. The QCA multiple scattering equations and dispersion relation are formulated in term of the T-matrix formulism and vector spherical wave function is utilized as basis functions [10].

Let $\overline{E}^{inc}(\overline{r})$ be the incident electric field in a medium with multiple species of N particles, and $\overline{E}^S_j(\overline{r})$ the scattered field from the jth

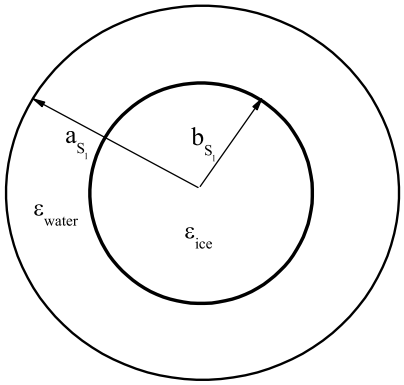

Figure 3. wet snow model.

particle. The total field at a point $\overline{r}$ is the sum of the incident field and the scattered fields from all the particles.

$$\overline{E}(\overline{r}) = \overline{E}^{inc}(\overline{r}) + \sum_{j=1}^{N} \overline{E}_j^S(\overline{r}) \tag{17}$$

the scattered field $\overline{E}_j^S(\overline{r})$ is related to the jth particle exciting field $\overline{E}^e(\overline{r})$ by

$$\overline{E}_j^e(\overline{r}) = \overline{\overline{T}}_j^{S_j}(\overline{r}) \cdot \overline{E}_j^e(\overline{r}) \tag{18}$$

where $\overline{\overline{T}}_j^{S_j}$ is the transition operator for particle j of S_j species. The exciting field for the jth particle can also be expressed as the total field less its own scattered field,

$$\overline{E}_j^e(\overline{r}) = \overline{E}^{inc}(r) + \sum_{l\neq j}^{L} \overline{E}_l^S(\overline{r}) = \overline{E}^{inc}(r) + \sum_{l\neq j}^{L} \overline{\overline{T}}_l^{S_l} \cdot \overline{E}_l^e(\overline{r}) \tag{19}$$

Under the quasicrystalline approximation, the integral equation for the conditional average of the jth particle exciting field, $\left\langle \overline{E}_j^e(\overline{r}) \right\rangle_j$, is

$$\left\langle \overline{E}_j^e(\overline{r}) \right\rangle_j = \overline{E}^{inc}(r) + \sum_{S_l=1}^{L} \int d\overline{r}_l \cdot g_{S_j S_l}(\overline{r}_l, \overline{r}_j) \cdot \overline{\overline{T}}_l^{S_j} \left\langle \overline{E}_l^e(\overline{r}) \right\rangle_l \tag{20}$$

where $\overline{\overline{T}}_l^{S_j} \left\langle \overline{E}_l^e(\overline{r}) \right\rangle_l$ is the field scattered by a scatterer of S_l species at $\overline{r}_l$ when excited by the field $\left\langle \overline{E}_l^e(\overline{r}) \right\rangle_l$.

For a plane electromagnetic wave normally incident upon a half-space of spherical scatterers, the incident field $\overline{E}^{inc}(\overline{r}) = \hat{y}e^{ikz}$ and the scattered field $\overline{T}_l^{S_l}\left\langle \overline{E}_l^e(\overline{r})\right\rangle_l$ can be expanded in vector spherical waves as [10]

$$\begin{aligned}\overline{E}^{inc}(\overline{r}) = e^{ikz_j}\sum_{n=1}^{\infty}\frac{i^n}{2}\sqrt{4\pi(2n+1)}[R_g\cdot\overline{M}_{1n}(k\overline{rr}_j) - R_g\cdot\overline{M}_{-1n}(k\overline{rr}_j)\\ +R_g\cdot\overline{N}_{1n}(k\overline{rr}_j) + R_g\cdot\overline{N}_{-1n}(k\overline{rr}_j)]\end{aligned} \tag{21}$$

$$\begin{aligned}\overline{\overline{T}}_l^{S_l}\left\langle \overline{E}_l^e(\overline{r})\right\rangle_l = \sum_{n=1}^{\infty}\sum_{m=-n}^{n}[T^{(M)_{S_l}}\cdot a_{mn}^{S_l}(z_l)\cdot\overline{M}_{mn}(k\overline{rr}_l)\\ +T^{(N)_{S_l}}\cdot b_{mn}^{S_l}(z_l)\cdot\overline{N}_{mn}(k\overline{rr}_l)]\end{aligned} \tag{22}$$

where $R_g\overline{M}_{mn}(k\overline{rr}_j)$ and $R_g\overline{N}_{mn}(k\overline{rr}_j)$ are regular vector spherical wave functions, and $\overline{M}_{mn}(k\overline{rr}_j)$ and $\overline{N}_{mn}(k\overline{rr}_j)$ are vector spherical functions with spherical Bessel function j_n replaced by spherical Hankel functions of the first kind h_n [10]. The symbol $\overline{rr}_j$ is used to denote the vector pointing from $\overline{r}_j$ to $\overline{r}$. The quantities $a_{mn}^{S_l}$, $b_{mn}^{S_l}$, are unknown expansion coefficients. The scattering coefficients $T_n^{(M)_{S_l}}$ and $T_n^{(N)_{S_l}}$ in Eq. (22), for coated spherical with outer radius a_{S_l}, inner radius b_{S_l}, core wavenumber k_{b_l}, and shell wavenumber k_{a_l}, are those of Mie scattering [11] (Fig. 3).

$$\begin{aligned}T_n^{(M)_{S_l}} = &-\{[\rho_{S_l}\cdot j_n(\rho_{S_l})]'\left[j_n(\zeta_{S_l}) + B_n^{S_l}\cdot y_n(\zeta_{S_l})\right]\\ &-\left[[\zeta_{S_l}\cdot j_n(\zeta_{S_l})]' + B_n^{S_l}[\zeta_{S_l}\cdot y_n(\zeta_{S_l})]\right]j_n(\rho_{S_l})\}\\ &/\{[\rho_{S_l}\cdot h_n(\rho_{S_l})]'\left[j_n(\zeta_{S_l}) + B_n^{S_l}\cdot y_n(\zeta_{S_l})\right]\\ &-\left[[\zeta_{S_l}\cdot j_n(\zeta_{S_l})]' + B_n^{S_l}[\zeta_{S_l}\cdot y_n(\zeta_{S_l})]\right]h_n(\rho_{S_l})\}\end{aligned} \tag{23}$$

$$\begin{aligned}T_n^{(N)_{S_l}} = &-\{[\rho_{S_l}\cdot j_n(\rho_{S_l})]'\zeta_{S_l}^2\left[j_n(\zeta_{S_l}) + A_n^{S_l}\cdot y_n(\zeta_{S_l})\right]\\ &-\left[[\zeta_{S_l}\cdot j_n(\zeta_{S_l})]' + A_n^{S_l}[\zeta_{S_l}\cdot y_n(\zeta_{S_l})]'\right]\rho_{S_l}^2\cdot j_n(\rho_{S_l})\}\\ &/\{[\rho_{S_l}\cdot h_n(\rho_{S_l})]'\zeta_{S_l}^2\left[j_n(\zeta_{S_l}) + A_n^{S_l}\cdot y_n(\zeta_{S_l})\right]\\ &-\left[[\zeta_{S_l}\cdot j_n(\zeta_{S_l})]' + A_n^{S_l}\cdot[\zeta_{S_l}\cdot y_n(\zeta_{S_l})]'\right]\rho_{S_l}^2\cdot h_n(\rho_{S_l})\}\end{aligned} \tag{24}$$

where

$$B_n^{S_l} = -\frac{[\xi_{S_l}\cdot j_n(\xi_{S_l})]'\cdot j_n(\eta_{S_l}) - [\eta_{S_l}\cdot j_n(\eta_{S_l})]'\cdot j_n(\xi_{S_l})}{[\xi_{S_l}\cdot y_n(\xi_{S_l})]'\cdot j_n(\eta_{S_l}) - [\eta_{S_l}\cdot j_n(\eta_{S_l})]'\cdot y_n(\xi_{S_l})} \tag{25}$$

$$A_n^{S_l} = -\frac{[\xi_{S_l} \cdot j_n(\xi_{S_l})]' \eta_{S_l}^2 \cdot j_n(\eta_{S_l}) - [\eta_{S_l} \cdot j_n(\eta_{S_l})]' \xi_{S_l}^2 \cdot j_n(\xi_{S_l})}{[\xi_{S_l} \cdot y_n(\xi_{S_l})]' \eta_{S_l}^2 \cdot j_n(\eta_{S_l}) - [\eta_{S_l} \cdot j_n(\eta_{S_l})]' \xi_{S_l}^2 \cdot y_n(\xi_{S_l})} \quad (26)$$

and $y_n(\cdot)$ is the spherical Neumann function. The symbols ρ_{S_l},ζ_{S_l},ξ_{S_l} and η_{S_l} are defined as $\rho_{S_l} = ka_{S_l}$, $\zeta_{S_l} = k_{a_l} a_{S_l}$, $\xi_{S_l} = k_{a_l} b_{S_l}$, $\eta_{S_l} = k_{b_l} b_{S_l}$, respectively.

To solve Eq. (20), assume the trial solutions

$$a_{\mu\nu}^{S_l}(z_j) = \alpha_{\mu\nu}^{S_j} e^{iKz_j} \quad (27)$$

$$b_{\mu\nu}^{S_l}(z_j) = \beta_{\mu\nu}^{S_j} e^{iKz_j} \quad (28)$$

with K being the effective propagation constant. The vector translational addition theorem is used to expand the spherical vector waves $M_{mn}(k\overline{rr}_l)$ and $N_{mn}(k\overline{rr}_l)$ about $\overline{r}_j$ as center in terms of the regular spherical waves $R_g\overline{M}_{mn}(k\overline{rr}_l)$ and $R_g\overline{N}_{mn}(k\overline{rr}_l)$. Equating terms with the same $R_g\overline{M}_{mn}(k\overline{rr}_l)$ and the same $R_g\overline{N}_{mn}(k\overline{rr}_l)$ gives the following relations [10].

$$K - k = -\frac{\pi i}{k^2} \sum_{S_l=1}^{L} \sum_{n=1}^{\infty} n_{S_l} \left[T_{S_l}^{(M)} \cdot X_{1n}^{S_l} + T_{S_l}^{(N)} \cdot Y_{1n}^{S_l} \right] (2n+1) \quad (29)$$

and

$$\begin{aligned} X_{1\nu}^{S_l} = & -2\pi \sum_{S_l=1}^{L} \sum_{n=1}^{\infty} \sum_{p=0}^{\infty} n_{S_l}(2n+1)[L_p(k,K|R_{S_jS_l}) + M_p(k,K|R_{S_jS_l})] \\ & \times \{T_n^{(M)S_l} \cdot X_{1n}^{S_l} \cdot a(1,n|-1,\nu|p) \cdot A(n,\nu,p) \\ & + T_n^{(N)S_l} \cdot Y_{1n}^{S_l} \cdot a(1,n|-1,\nu|p,p-1) \cdot B(n,\nu,p)\} \quad (30) \\ Y_{1\nu}^{S_l} = & -2\pi \sum_{S_l=1}^{L} \sum_{n=1}^{\infty} \sum_{p=0}^{\infty} n_{S_l}(2n+1)[L_p(k,K|R_{S_jS_l}) + M_p(k,K|R_{S_jS_l})] \\ & \times \{T_n^{(M)S_l} \cdot X_{1n}^{S_l} \cdot a(1,n|-1,\nu|p,p-1) \cdot A(n,\nu,p) \\ & + T_n^{(N)S_l} \cdot Y_{1n}^{S_l} \cdot a(1,n|-1,\nu|p) \cdot B(n,\nu,p)\} \quad (31) \end{aligned}$$

where the coefficients $X_{1\nu}^{S_l}$ and $Y_{1\nu}^{S_l}$ are related to the trial solutions $\alpha_{1\nu}^{S_l}$ and $\beta_{1\nu}^{S_l}$ by, respectively

$$X_{1\nu}^{S_j} = \frac{2i^{-\nu}}{\sqrt{4\pi(2\nu+1)}} \alpha_{1\nu}^{S_j} \quad (32)$$

$$Y_{1\nu}^{S_j} = \frac{2i^{-\nu}}{\sqrt{4\pi(2\nu+1)}}\beta_{1\nu}^{S_j} \tag{33}$$

The expressions for $a(m,n|\mu,\nu|p)$, $a(m,n|\mu,\nu|p,q)$, $A(n,\nu,p)$, $B(n,\nu,p)$ and quantities $L_p(k,K|R_{S_jS_l})$ and $M_p(k,K|R_{S_jS_l})$ are all given in Ref. [7].

Eqs. (30)–(31) form a system of simultaneous homogeneous equations for the unknown $X_{1n}^{S_l}$ and $Y_{1n}^{S_l}$. For nontrivial solution, the determinant of the coefficients must vanish. The requirement for the vanishing of the determinant gives an equation for efficient wavenumber K. Thus, the effective propagation constant K is then calculated by searching in the complex plane such that the determinant of Eqs. (30)–(31) vanishes. Numerical algorithm about the effective propagation constant K can be referred [7].

3. NUMERICAL RESULTS AND DISCUSS

We illustrate the brightness temperature for passive microwave remote sensing of wet snow. The wet snow and moist soil temperatures are all $260K$. Frequencies are at 18.7 GHz and 36.5 GHz. The rough surface parameters are rms height of 0.4 mm, and correlation length 2.8 mm. The permittivity, for water is $\varepsilon_{water} = 68.44 + i35.39$, for ice grain is $\varepsilon_{ice} = 3.15 + i0.002$ at 18.7 GHz and $\varepsilon_{ice} = 3.15 + i0.0039$ at 36.5 GHz, for wet snow is $\varepsilon_1 = 1.43 + i0.002$, and for moist soil is $\varepsilon_g = 15.34 + i3.66$, except stated otherwise. Fractional volume is 30%, and snow layer thickness is 50 cm. The observation angle is 30 degrees. The stickiness parameter is $\tau = 0.1$.

3.1. Comparison of Brightness Temperatures between Rough and Flat Surfaces for Small Grain Size Case

In Figs. 4 to 7 we compare the brightness temperatures between rough and flat surfaces. To show the roughness effects, we first choose coated dielectric grain and core ice diameters to be 0.2 mm and 0.1999999 mm respectively in Figs. 4 and 5 so that volume scattering effects are small.

Fig. 4 shows the brightness temperature at 18.7 GHz as functions of angle in air region. For both horizontal and vertical polarizations, brightness temperature for rough surface is smaller than that of flat surface, which shows that contribution from rough surface is smaller than that from flat surface. This is because multiple scattering occurring along the rough surface will enhance the scattering wave extinction so as to reduce the scattering from rough surface. Meanwhile, for horizontal polarization, when observation angle is larger

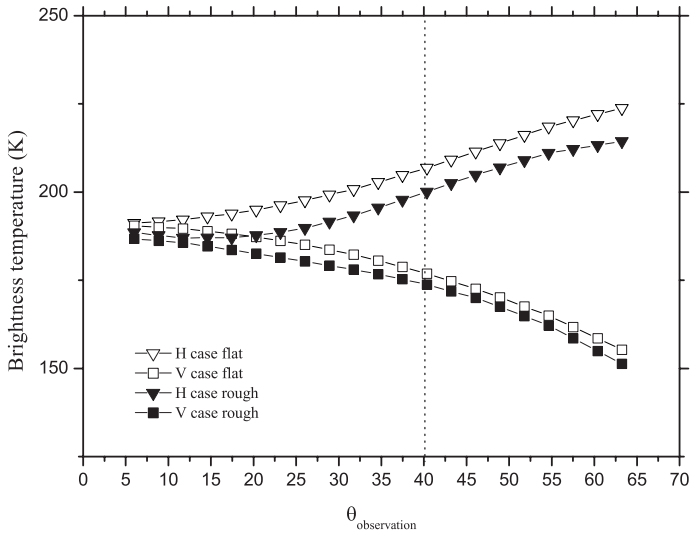

Figure 4. Comparison between rough and flat surface at different observation angles, $f = 18.7\,\mathrm{GHz}$.

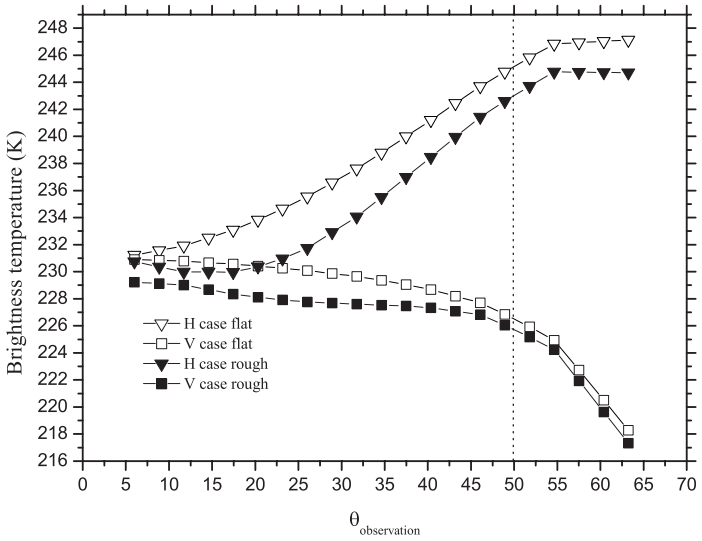

Figure 5. Comparison between rough and flat surface at different observation angles, $f = 36.5\,\mathrm{GHz}$.

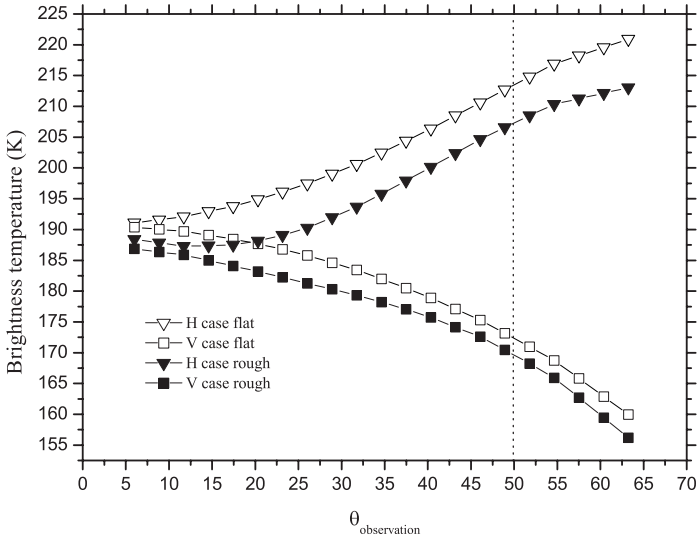

Figure 6. Comparison between rough and flat surface at different observation angles, $f = 18.7\,\text{GHz}$.

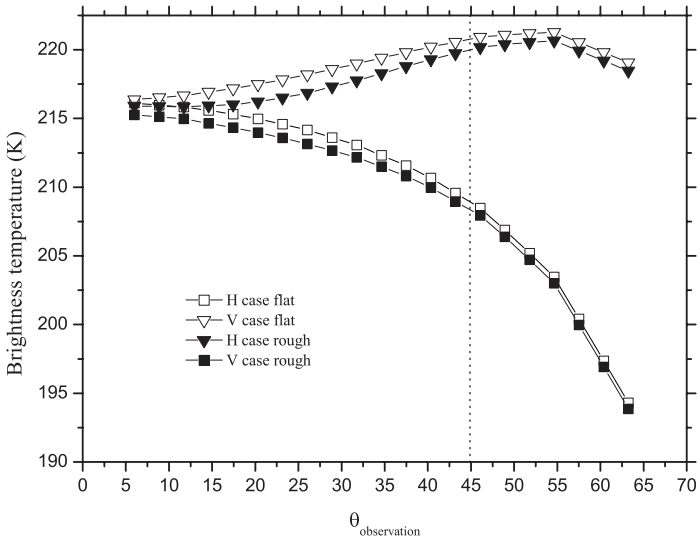

Figure 7. Comparison between rough and flat surface at different observation angles, $f = 36.5\,\text{GHz}$.

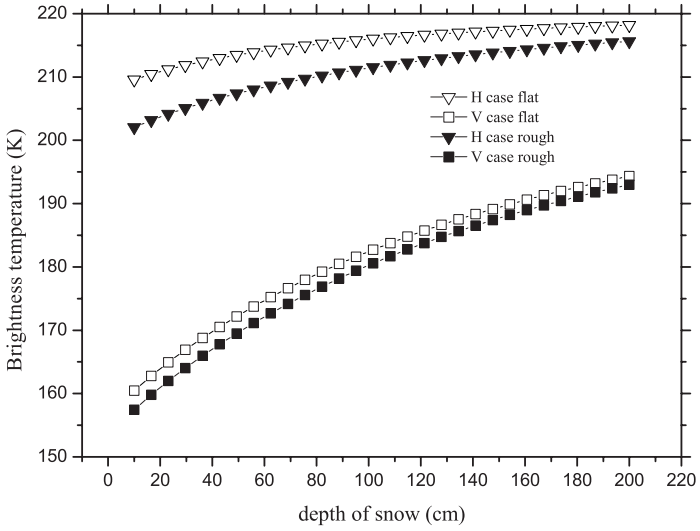

Figure 8. Comparison between rough and flat surface at different snow depths, $f = 18.7\,\text{GHz}$.

than 40°, the difference of brightness temperatures between rough and flat surfaces becomes smaller with increasing observation angle. On the other hand, at the higher frequency of 36.5 GHz in Fig. 5, volume scattering becomes important. When observation angle is larger than 50°, the difference of brightness temperatures between rough and flat surfaces becomes even smaller with increasing observation angle.

Figs. 6 and 7 compare results of flat and rough surfaces as functions of observation angle for the case of larger coated dielectric grain and core, whose sizes of diameter are 0.6 mm and 0.5999999 mm, respectively. Volume scattering becomes important at 18.7 GHz. When observation angle is bigger than 50°, the difference of brightness temperatures between rough and flat surfaces becomes even smaller with increasing observation angle. In particularly, at high frequency of 36.5 GHz, the effect on rough surface's roughness on the reduction the brightness temperatures will be furthermore pronounced. Thus when observation angle is bigger than 45°, the difference of brightness temperatures between rough and flat surfaces will be decreased for both horizontal and vertical polarizations, and even be the same as for horizontal polarization.

Figs. 8 and 9 compare results of flat and rough surfaces as functions of depth of snow; the sizes of coated dielectric grain and core ice are the same as above. At 18.7 GHz, with increasing depth of snow,

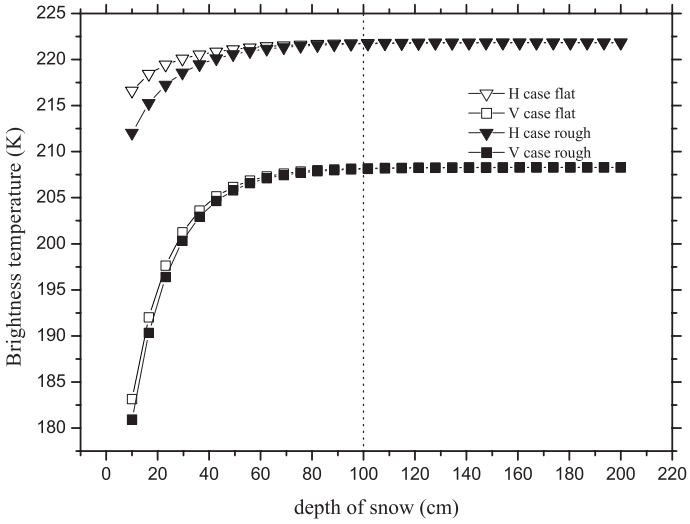

Figure 9. Comparison between rough and flat surface at different snow depths, $f = 36.5\,\text{GHz}$.

contribution from volume scattering to brightness temperature will be enhanced, and contribution from surface scattering will be reduced, so the difference of brightness temperatures between rough and flat surfaces is smaller for both vertical and horizontal polarization. In Fig. 9, we see that at high frequency of 36.5 GHz, saturation occurs at large snow depth. Volume scattering becomes dominant and rough surface scattering has a negligible effect.

3.2. Brightness Temperature Variations with Grain Size, Observation Angle and Snow Depth

In this section, we study brightness temperature from wet snow with increasing coated grain size. Figs. 10 and 11 show the angular variations of brightness temperature for several coated dielectric grain sizes of diameter. The brightness temperature decrease with increasing grain size. This is because with increasing coated grain size, scattering among the coated grains will enhance. Meanwhile, emission from the ground is scattered and thus unable to reach the air region, which accounts for the decrease in brightness temperature.

Figs. 12 and 13 show that for small coated dielectric grain size, brightness temperature will increase with increasing thickness of the snow layer, up to saturation at 38.7 GHz. For larger grain size, brightness temperature will decrease with increasing snow depth at

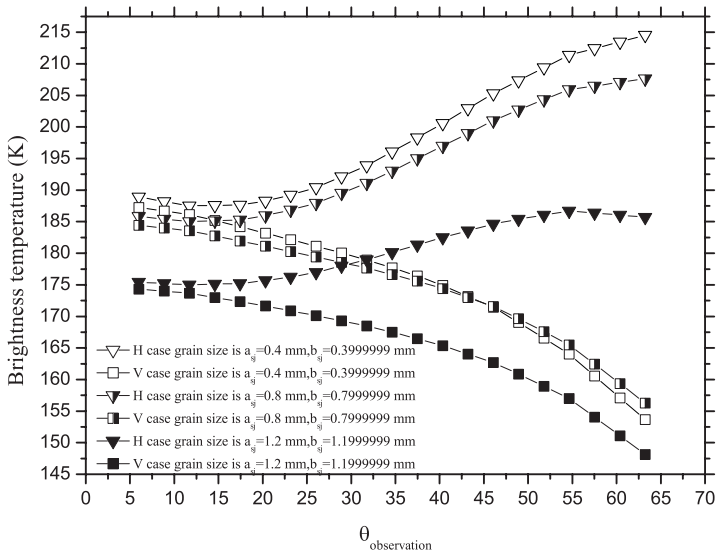

Figure 10. Varying coated dielectric grain size and as a function of observation angle, $f = 18.7\,\mathrm{GHz}$.

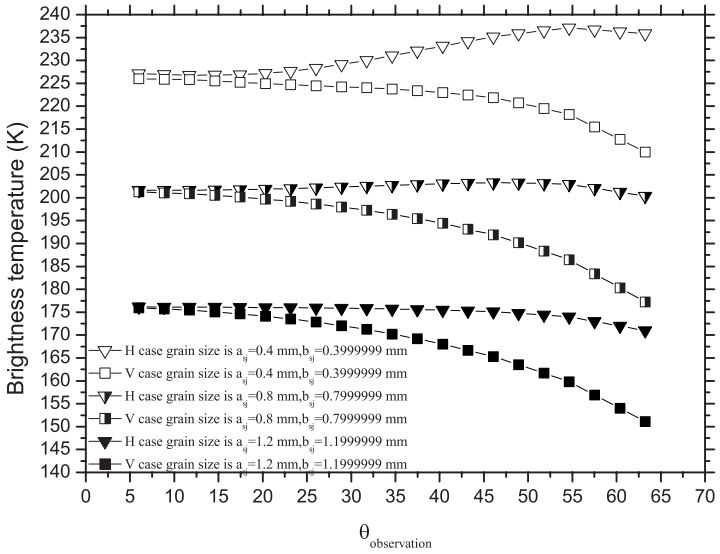

Figure 11. Varying coated dielectric grain size and as a function of observation angle, $f = 36.5\,\mathrm{GHz}$.

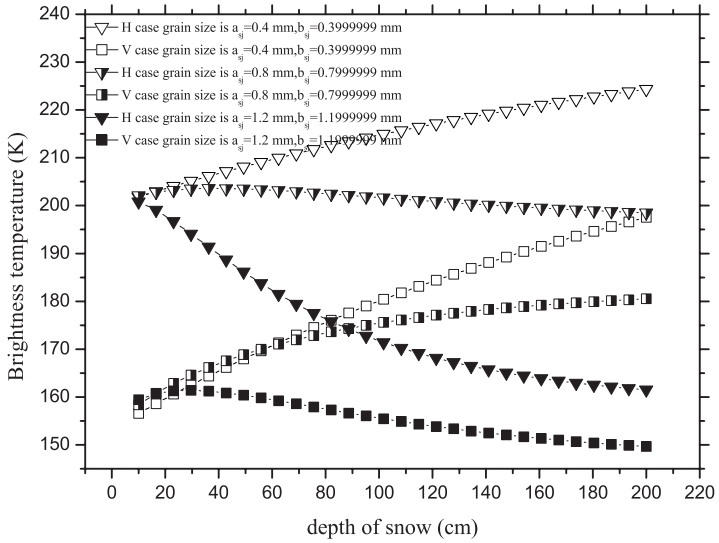

Figure 12. Varying coated dielectric grain size and as a function of snow depth $f = 18.7\,\mathrm{GHz}$.

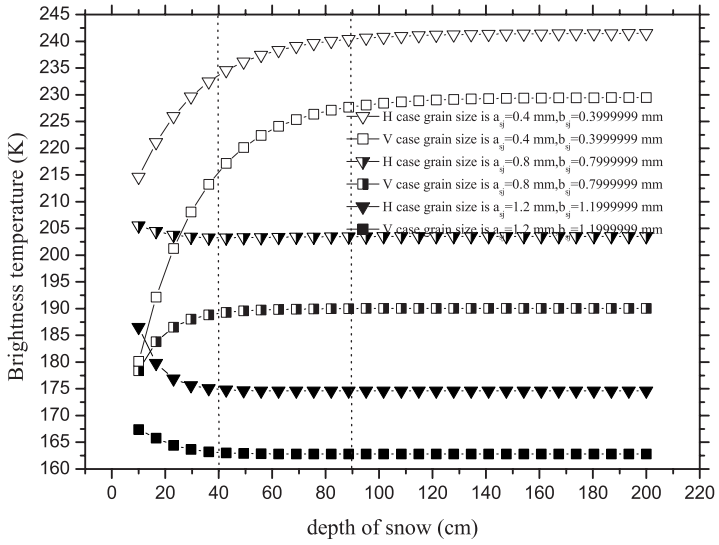

Figure 13. Varying coated dielectric grain size and as a function of snow depth $f = 36.5\,\mathrm{GHz}$.

18.7 GHz. For 36.5 GHz, saturation effects occur as functions of snow depth.

3.3. Brightness Temperature Variations with Proportion between Inner and Outer Radius of Coated Grain, Observation Angle and Snow Depth

In this section, we study brightness temperature from wet snow with varying proportion between outer and inner radius of coated grain. Outer radius of coated grain is fixed at 0.6mm, inner radius of coated grain is varying with three cases, 0.5 mm, 0.5999 mm and 0.5999999 mm, respectively. Fig. 14 and Fig. 15 show that with increasing inner radius of coated grain (ice), the brightness temperature from wet snow will enhance for both 18.7 GHz and 36.5 GHz. The reason is that with decreasing inner radius of coated grain (ice), the thickness of the water thin film surrounded ice will increase, so does the wet snow's absorptivity; on the other hand, since the outer radius of coated grain is unvaried, scattering among the coated grains will remain almost unchanged in this wet snow model. In this way, wet snows emissivity will enhance, and brightness temperature will increase.

Fig. 16 and Fig. 17 show that with increasing depth of wet snow, brightness temperature from wet snow will enhance for both 18.7 GHz and 36.5 GHz cases. Meanwhile, saturation effects occur when the proportion between outer and inner radius is 0.6/0.59 for both 18.7 GHz and 36.5 GHz, which means brightness temperature from wet snow for both horizontal and vertical polarizations will be unvaried with increasing depth of wet snow. This saturation also occurs for other two proportion cases at 36.5 GHz when the depth of wet snow exceeds 50 mm.

4. SUMMARY

Volume scattering and rough surface scattering effects in passive microwave remote sensing of wet snow are studied in this paper. The volume scattering model is based on DMRT theory with QCA for densely distributed sticky coated dielectric particles. The rough surface bistatic scattering and emission are modeled by the NMM3D. The bistatic scattering coefficients and emissivities of rough surfaces are utilized as the boundary conditions for the DMRT. Wet snow model is adopted in this paper. The results for a layer of wet snow over a moist rough ground at 18.7 GHz and 38.5 GHz are discussed.

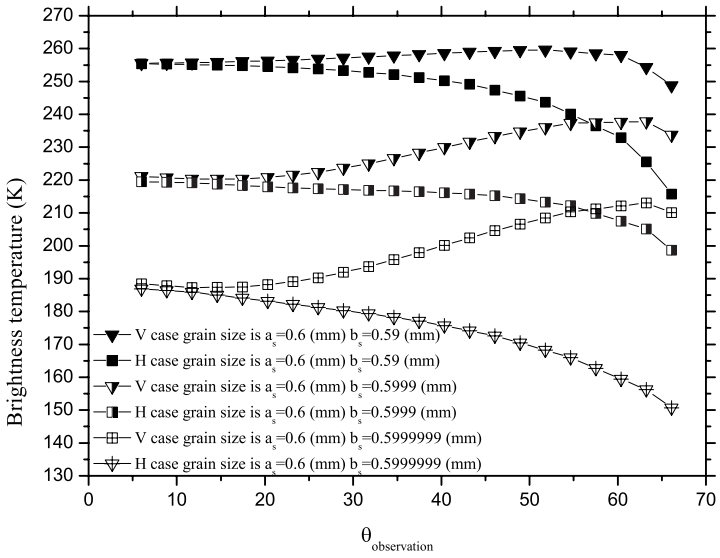

Figure 14. Varying proportion between inner and outer radius of coated dielectric grain as functions of observation angle, $f = 18.7\,\mathrm{GHz}$.

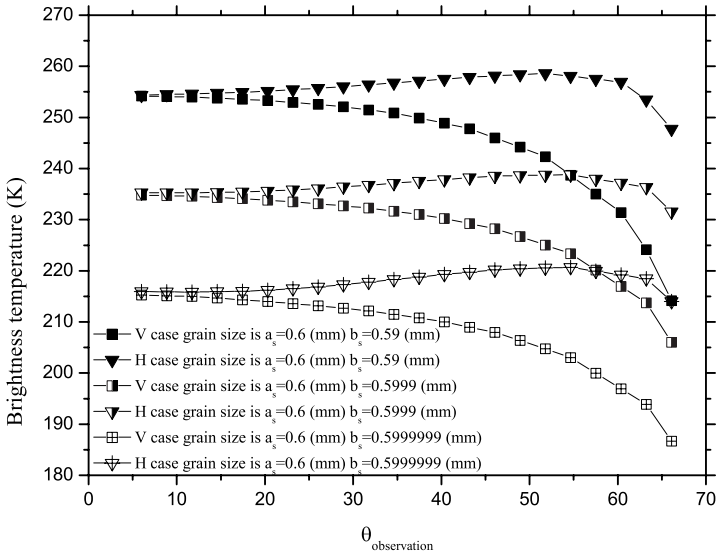

Figure 15. Varying proportion between inner and outer radius of coated dielectric grain as functions of observation angle, $f = 36.5\,\mathrm{GHz}$.

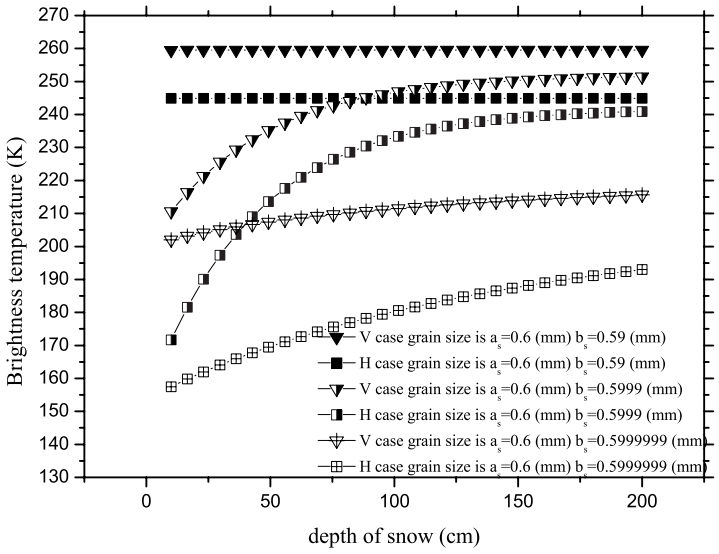

Figure 16. Varying proportion between inner and outer radius of coated dielectric grain as functions of snow depth $f = 18.7\,\mathrm{GHz}$.

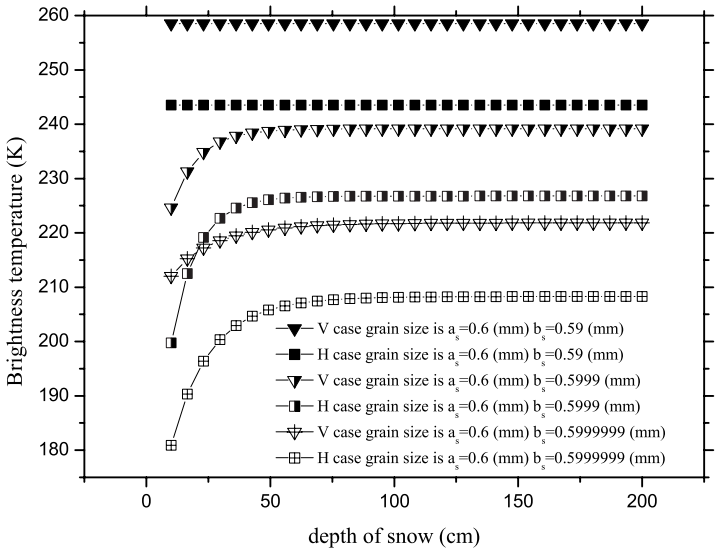

Figure 17. Varying proportion between inner and outer radius of coated dielectric grain as functions of snow depth $f = 36.5\,\mathrm{GHz}$.

ACKNOWLEDGMENT

The research in this paper was supported by RGC Central Allocation Grant 8730017 of Hong Kong and NASA of USA and the Electromagnetic Academy at Zhejiang University. The author acknowledges stimulating discussions with Prof. Leung Tsang of Electrical Engineering at the University of Washington.

REFERENCES

1. Lam, C. M. and A. Ishimaru, "Mueller matrix calculation for a slab of random medium with both random rough surfaces and discrete particles," *IEEE Transactions on Antenna and Propagation*, Vol. 42, No. 2, 145–156, Feb. 1994.
2. Zhou, L., L. Tsang, and D. Chen, "Polarimetric microwave remote sensing of wind vectors with foam covered rough ocean surfaces," *Radio Science*, Vol. 38, No. 4, DOI, 10.1029/2002RS002764, August 2003.
3. Tsang, L., J.A. Kong, K. H. Ding, and C. O. Ao, *Scattering of Electromagnetic Waves*, Vol. 2, Numerical Simulations, Wiley Interscience, 2001
4. Tsang, L. and J. A. Kong, *Scattering of Electromagnetics Waves*, Vol. 3, Advanced Topics, Wiley Interscience, New York, 2001.
5. Zhou, L., L. Tsang, V. Jandhyala, Q. Li, and C. H. Chan, "Emissivity simulations in passive microwave remote sensing with 3-D numerical solutions of Maxwell equations," *IEEE transactions on Geoscience and Remote Sensing*, Vol. 42, No. 8, 1739–1748, August 2004.
6. Arslan, A. N., H. Wang, J. Pulliainen, and M. Hallikainen, "Effective permittivity of wet snow using strong fluctuation theory," *Journal of Electromagnetic Waves and Applications*, Vol. 15, 53–55, 2001.
7. Ding, K. H. and L. Tsang, "Effective propagation constants and attenuation rates in media of densely distributed coated dielectric particles with size distribution," *Journal of Electromagnetic Waves Application*, Vol. 5. No. 2, 117–142, 1991.
8. Ding, K. H., L. M. Zurk, and L. Tsang, "Pair distribution functions and attenuation rates for sticky particles in dense media," *Journal of Electromagnetic Waves Application*, Vol. 8, 1585–1604, Dec. 1994.
9. Tsang, L., J. A. Kong, and K. H. Ding, *Scattering of*

Electromagnetics Waves, Vol. 1, Theories and applications Wiley Interscience, New York, 2000.

10. Tsang, L., J. A. Kong, and R. T. Shin, *Theory of Microwave Remote Sensing*, Wiley Interscience, New York, 1985.
11. Bohren, C. F. and D. R. Huffman, *Absorption and Scattering of Light by Small Particles*, John Wiley & Sons, New York, 1983.